HiSST: 2nd International Conference on
High-Speed Vehicle Science Technology
11–15 September 2022, Bruges, Belgium

Aerodynamics Analysis of Vehicle Moving in a Tube

Mohammed Mahdi Abdulla [1], Seraj Alzhrani [2], Khalid A. Juhany [3]

Abstract

High-speed moving vehicles in a tube with pressures similar to those experienced in aircraft at their maximum altitude are investigated and presented. Although the concept resembles Hyperloop, the pressure level investigated here is much higher and safer than that suggested by the Hyperloop, and therefore, the system design is markedly different. The vehicle's aerodynamic drag reduces with lower operating pressures, blockage ratios, and flow Mach number. Most of the publications addressed and studied the blocked model. However, the role of flow ingestion is not well studied. This paper analyzed the ingestion effect on the flow field, power, and drag using multi-dimensional analysis utilizing the Method of Characteristics (1-D) and Unsteady Reynolds Averaged Navier Stokes (URANS) with $k-\omega$ SST turbulence model for the 2-D and 3-D numerical models. A comparison between the blocked and ingested models was performed for various ranges of Mach number (0.3 to 0.8) and blockage ratios (0.3 to 0.7) to assess the performance of a wide range of design spaces. The attained results have shown a significant reduction of piston effect, elimination of chocking condition, and providing the required thrust levels to propel the vehicle along the tube. Interestingly, the analysis revealed a power savings of approximately 90% when ingestion was employed with a vehicle speed corresponding to M=0.6 at an operating pressure of 10 kPa.

Keywords: *Hyperloop, Numerical Scheme, Method of Characteristics, 1-D viscous compressible model, Ingested model.*

Nomenclature

A_v	=	Vehicle area
A_{vw}	=	Area between pod and tube
A_e	=	Nozzle exit area
A_{inlet}	=	Area at compressor inlet
A^*_{nozzle}	=	Nozzle area corresponding to M=1
a	=	Speed of sound
C_p	=	Specific heat at constant pressure
C_f	=	Skin friction coefficient
c_H	=	Convection heat transfer coefficient
D	=	Drag force
D_P	=	Pod diameter
dt	=	Time step
Kn	=	Knudsen Number
L	=	Vehicle's length
M	=	Mach Number
$\dot{m}$	=	Mass flow rate
p	=	Operating pressure
P_∞	=	Free stream pressure
P_e	=	Nozzle Exit pressure
q	=	Tube heat transfer rate
q_v	=	Vehicle heat transfer rate
R	=	Gas constant
Re	=	Reynolds number
T_w	=	Wall temperature
u_s	=	Velocity at point A as in Fig. (2)
V_j	=	Jet velocity
V_∞	=	Free stream velocity
x,y,z	=	Coordinate system
β	=	Blockage ratio $=\frac{A_v}{A_{tube}}$
γ	=	$\frac{c_p}{c_v} = 1.4$ for ideal air
ρ	=	Flow density
τ_w	=	Wall shear stress

[1] *PhD Student, Aerospace Engineering Department, King Abdulaziz University, Jeddah 21589, Saudi Arabia*
[2] *Lecturer, Aerospace Engineering Department, King Abdulaziz University, Jeddah 21589, Saudi Arabia*
[3] *Chairman, Aerospace Engineering Department, King Abdulaziz University, Jeddah 21589, Saudi Arabia*

1 Introduction

The transportation sector has a vital role in human life and the global economy. Moving to more efficient, safe, reliable, accessible, sustainable, and cost-effective transportation means is essential since technology, innovative ideas, and manufacturing capabilities have improved substantially in the last few decades. Elon Musk, in his white paper [1] was paved the roadmap for the development of high-speed vehicles moving in a low operating pressure tube. Historically, the concept of evacuated tube transportation has emerged and was registered as a patent in the United States in 1950 [2],1965 [3]. The European initiative for evacuated tube technologies (et3) was also an important milestone in 1999 [4]. High-speed traveling vehicles in an evacuated tube and a low-pressure environment have attracted global attention as an upgrade of high-speed land transportation [5], [6]. Traveling at a pressure level of 100 Pascals, equivalent to traveling at 150,000 ft, requires a vehicle design with space-rated standards and raises great concerns for passengers' safety. The pressure levels promoted in the current study are similar to pressure conditions experienced by jet aircraft at their maximum flight altitude. Airliners flying today reach 45,000 feet, while business jets can reach 51,000 feet [5]. The lowest acceptable pressure employed in this work would be that equivalent to an altitude of 60,000 ft of the flight-proven Concorde (10 kPa).

The aerodynamic phenomenon caused by the movement of the vehicle traveling in a tube which includes the propagation of compression waves, and expansion waves, were studied theoretically [7]–[9] and experimentally [10]–[12]. Computational Fluid Dynamics (CFD) has been increasingly used in simulating and developing high-speed vehicles [13]–[25]. Like the tube, the tunnel introduces a blockage effect highlighted as a constraint to the train's performance and the tube operating pressure as the flow tends to be choked [7], [26]–[28]. Once the choking phenomenon occurs, the adverse pressure gradient is evident, and additional power is required to overcome the generated drag acting on the vehicle [29]. Sucking such a flow from the front of the vehicle to its rear using an air axial compressor can mitigate the choked flow effect (Kantrowitz limit) and allow the vehicle to travel fast and efficiently [30], [31]. To the author, no experimental data exist on the vehicle traveling in a long tube at low-pressure levels, but the work of Fukuda et al provides a field measurement on Shinkansen train system that allows them to validate their simplified 1-D model using the method of characteristics to study the compression wave moving in the tunnel [32]–[34].

The current work defines the analysis of the flow air-breathing effect on the flow field and power consumption using URANS model. The K- ω SST turbulent model was used to investigate the blocked and ingested models. Fig. (1) shows the schematic of the vehicle-tube system with an axial air compressor driven by an electric motor installed in the front of the vehicle. Jet nozzle flow aimed to generate the required thrust. The proposed system is environmentally friendly, clean, and safe.

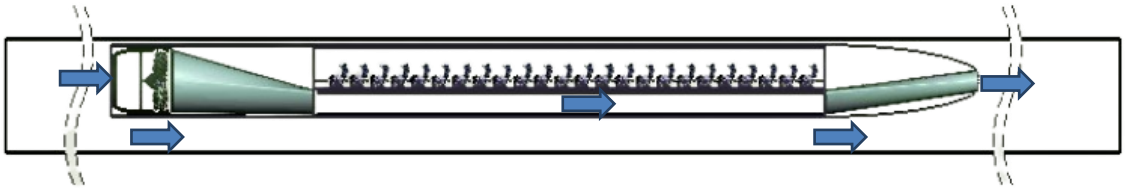

Figure 1. Vehicle-tube system with air ingestion

2 Vehicle-Tube System Design:

Current electrical driven aero-engines technologies like the Efanx, which is a joint program between Airbus, Rolls-Royce and Siemens [35], has made the current proposed concept more feasible. Many challenges appeared during this journey since all published works studied the blocked model as shown in Fig. (2a). Limited studies have considered the air-breathing effect in such a closed environment

system [36]. Allowing flow to pass through the pod will generate thrust, significantly mitigate the piston effect, and reduce the choking condition. The thrust force generated by the system is given by:

$$Thrust = \dot{m}(V_j - V_\infty) + (P_e - P_\infty)A_e \quad (1)$$

In this work, the scope of analysis did not consider the internal flow in the duct, the mass flow inlet to the pod, and continuity enables us to study the overall system performance assuming no choking occurs inside the nozzles and duct system inside the pod given that the inlet to exit nozzle area ratio :

$$\frac{A_{inlet}}{A^*_{nozzle}} = \frac{1}{M}\left(\frac{1+\frac{\gamma-1}{2}M^2}{\frac{\gamma+1}{2}}\right)^{\frac{\gamma+1}{2(\gamma-1)}} \quad (2)$$

the critical area A* represents the nozzle area where the corresponding exit Mach number equals 1 at this section.

2.1 Problem Description

Fig. (2) presents the simplified 2-D physical domain for the two cases (i.e., the blocked model and the ingested model). The blocked model is defined as a solid surface where no flow is allowed to be breathed by the vehicle. This stimulates the piston effect phenomenon to occur due to the presence of the compression wave, causing a deceleration of the vehicle due to the tremendous amount of drag force encountered by the system. Introducing an air-breathing system by a fan /compressor module will mitigate the piston effect and help decrease the pressure levels inside the tube, so the pressure drag decreases remarkably. A domain length of 20 km is applied during the analysis of both cases.

It is important to investigate the Knudsen Number (kn) which is defined as the particle mean free path ratio over the characteristic length scale. Flow regimes could be continuum or discrete based on Knudson Number. If kn >0.01, the flow is no longer a continuum [5]. The physical Knudsen Number k_{ns}, designated by the particle mean free path and the characteristic length scale where the numerical Knudsen Number k_{nc}, correlates the mean free path over the cell size. The numerical Knudsen Number controls the final CFD result, specifically with a lower Reynolds Number encountered in low operating pressure. Finally, we may have that k_n is a function of k_{ns} and k_{nc}[37].

$$Kn_{s,n} = \sqrt{\frac{\gamma\pi}{2}}\frac{Ma}{Re_{s,c}} \quad (2)$$

The numerical Knudsen Number is calculated with the fine grid considering at y+=1, and equal to 0.008, which proves the flow's continuum assumption.

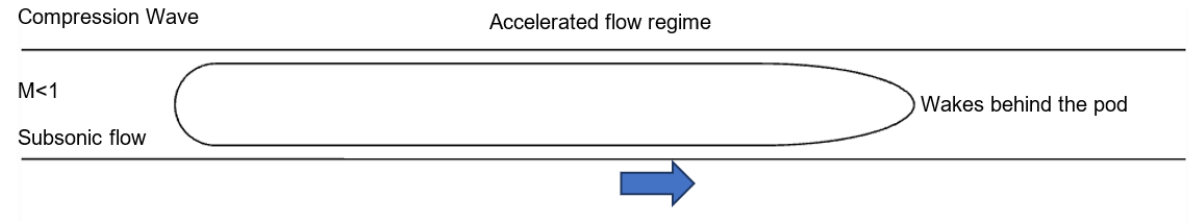

(a)

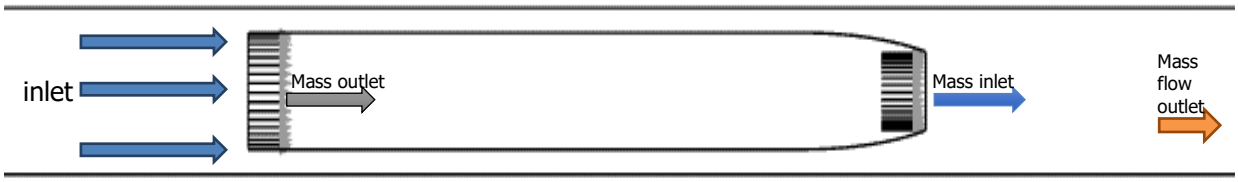

(b)

Figure 2. (a) Blocked model (b) Ingested model schematics

2.2 1-D Aerodynamics Analysis

The simplified 1-D model provides low-cost and rapid development for the vehicle-tube design. The blockage ratio and the operating conditions (Mach, Pressure) are essential parameters for the system. The moving duct concept developed by Hammit [38]–[40], and Woods [41] uses an incompressible flow model. This section extends the work of Hammit and Woods to include flow compressibility, skin friction and heat transfer to build a simplified 1-D compressible method. The flow domain is divided into two fields:

a) *Near-field*: where the vehicle shape effect is studied. The flow is steady, and the pressure, velocity, are evaluated in the narrow flow passages between the moving vehicle and the tube.

b) *Far-field:* the flow field pressure propagations confined within tube walls and dissipated by the friction and the amount of heat transferred. Here the 1-D method of characteristics (MoC) could be utilized.

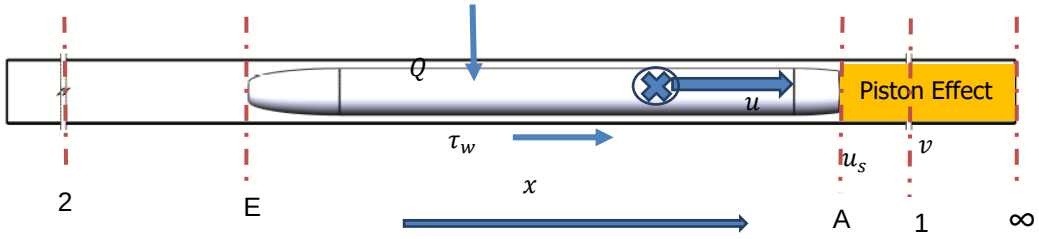

Figure 3. Schematic of pod motion in a tube

From the continuity, momentum, and energy equations for a steady variable area duct, we can have:-

$$\begin{bmatrix} \frac{dv}{dx} \\ \frac{dp}{dx} \\ \frac{dT}{dx} \end{bmatrix} = \begin{bmatrix} \frac{1}{v} & \frac{1}{p} & -\frac{1}{T} \\ \rho v & 1 & 0 \\ v & 0 & c_p \end{bmatrix}^{-1} \begin{bmatrix} -\frac{1}{A}\frac{dA}{dx} \\ -\frac{1}{2}\rho u^2 c_f \frac{4}{d(1-\beta)} + \frac{1}{2}\rho v^2 c_f \frac{4}{d}\frac{\beta^{\frac{1}{2}}}{(1-\beta)} \\ \frac{2c_f}{v(1-\beta)}\left(u^2 u_s - u^3 + u c_p (T_w - T)\right) \end{bmatrix} \tag{2}$$

The far-field, the unsteady flow equations are adopted:

$$\begin{cases} \frac{\partial \rho}{\partial t} + \rho \frac{\partial u}{\partial x} + u \frac{\partial \rho}{\partial x} = 0 \\ \frac{\partial u}{\partial t} + u \frac{\partial u}{\partial x} + \frac{1}{\rho}\frac{\partial p}{\partial x} + \frac{4\tau_w}{\rho d} = 0 \\ \frac{\partial \rho}{\partial t} + u \frac{\partial p}{\partial x} - a^2\left(\frac{\partial \rho}{\partial t} + u \frac{\partial \rho}{\partial x}\right) = (\gamma - 1)\frac{4}{d}(q_w + 4\tau_w) \end{cases} \tag{3}$$

The friction force $F = \frac{2c_f}{d}u^2$ and q is the heat flux. The characteristic lines are defined by $\mathrm{dx/dt} = u \pm a$, and the pathline is along u. The change in velocity due to viscous and heat transfer effects is given by:

$$du = \mp \frac{2}{\gamma - 1} da + \left[\pm \frac{4\gamma q_w}{\rho d a} - \frac{4\tau_w}{\rho d}\left(1 \mp \frac{u}{a}\right) + \frac{a^2}{\gamma}\frac{\partial}{\partial x}\left(\frac{s}{R}\right)\right] dt \tag{4}$$

The entropy change is given by:

$$(ds)_{path} = \frac{uF + q}{T}(dt)_{path} \tag{5}$$

Where the local velocity $u = \frac{1}{2}(R^+ - R^-)$, and the local speed of sound $a = \frac{\gamma - 1}{4}(R^+ + R^-)$. Furthermore, the wave location is given by:

$$x - x_p(t_p) = \left[a_a + \frac{\gamma + 1}{2} u_p(t_p)\right](t - t_p) \tag{6}$$

Where $x_p(t_p)$ is wave location in time t_p.

2.3 The Grid and Boundary Conditions

Three grid levels for the blocked and the ingested models are generated by using ICEM CFD. Fig. (4) & (5) present the grid for the two cases under investigation.

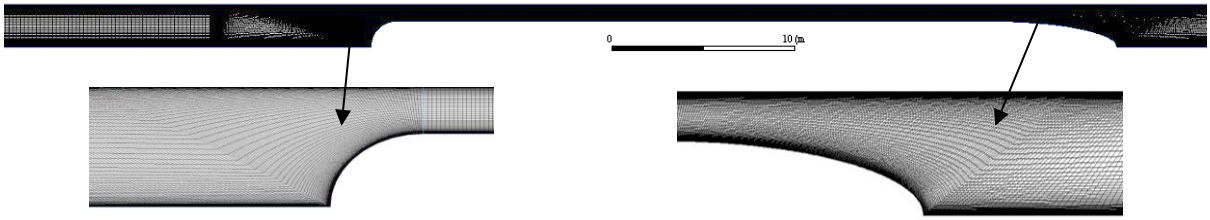

Figure 4. Blocked model grid

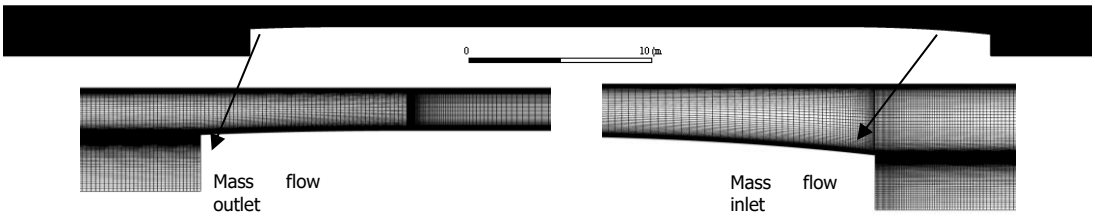

Figure 5. Ingested model grid

Boundary conditions: the farfield boundaries defined for inlet/outlet tube portals, moving wall corresponding to flow Mach Number is defined to simulate relative flow between tube and vehicle, vehicle walls are stationary. Mass flow outlet and inlet boundary conditions were defined for vehicle inlet and outlet, respectively. A grid convergence study was performed to validate the results for both blocked and ingested models. Fine grid results were used for drag force comparison.

Table 1 Grid Convergence Study

	Mesh size		Drag (N)		Difference from the fine grid (%)	
	Ingested	Blocked	Ingested	Blocked	Ingested	Blocked
Coarse	536,800	661,700	4660	51440	-6%	5%
Medium	1,687,500	1,870,125	5112	47300	3%	-3%
Fine	2,318,600	2,729,400	4980	48900	-	-

3 Results

Shock train and compression waves are the dominating phenomena for the blocked model of high-speed vehicles moving in closed environments. A simplified model was used to highlight the effect of air breathing through the vehicle towards the jet nozzle to contribute to the system's propulsion was introduced. The following sections will highlight the effect of flow ingestion on the flow field, drag levels, and power consumption. Performing a multi-dimensional aerodynamics analysis provides a detailed study of the vehicle-tube flow field.

3.1 1-D Method of Characteristics (MoC) results for the blocked model

The method of characteristics described in section 2.2 provides a rapid solution to predict the pressure wave propagation within the confined tube system. A verification with URANS $k-\omega$ SST solution of the 2-D blocked model is shown in Fig. (6-a), proving a good agreement for the time series results for the pressure wave propagations along the tube at t=1 and t=2.5 sec.

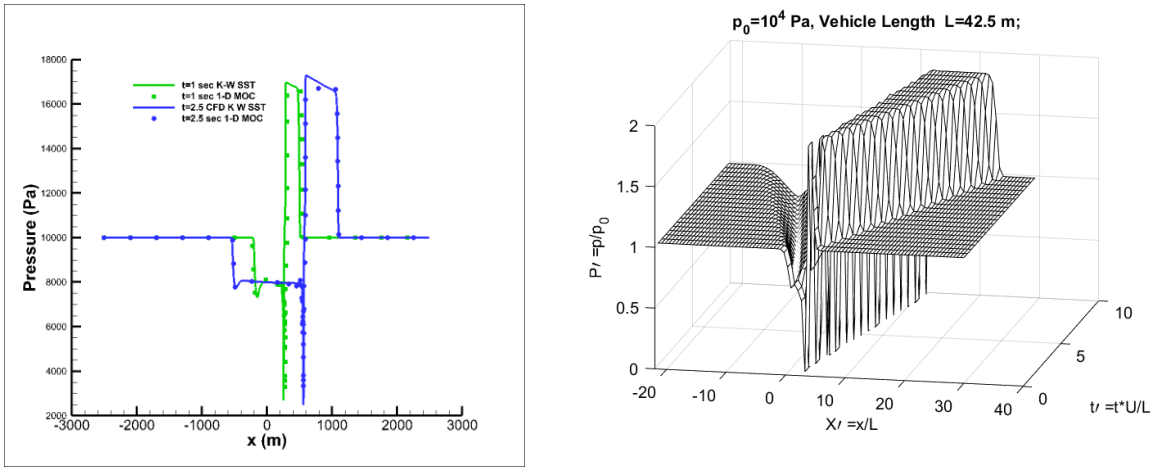

(a) **(b)**

Figure 6. Pressure wave propagation (a) along x-coordinates at t= 1, 2.5 sec, (b)wave propagation in x-space and time, $\beta = 0.56$

Fig. (6-b) illustrates a three-dimensional plot where the x-axis shows the non-dimensional length (tube length normalized with vehicle length), and the y-axis shows the non-dimensional time (flow time normalized with vehicle speed and length). In addition, the z-axis presents the pressure ratio (static pressure normalized with operating pressure). It is evident that the pressure wave keeps propagating with time and space. Vehicle movement along the tube induced the pistopn effect and the compression wave keep propagating with space and time, also the aftbody wakes and expansion waves reduces the pressure after the vehicle. Referance frame is attched to vehicle in this analysis. We also notice pressure reduces remarkably due to the wake and expansion of the flow behind the vehicle as shown in Fig. (7a, 8a).

3.2 Effect of ingestion on flow field:

The static pressure contours for the operating pressure levels of 10 kPa and M=0.6 are provided in Fig. (7). For the two cases (blocked and ingested models), at the fine grid levels, the ingested model (Fig. 7-b) shows mitigation of the piston effect, choking condition, and the wakes after the body (Fig. 7-a). The vehicle generates thrust from the internal flow duct system that allows ingesting the flow through the pod.

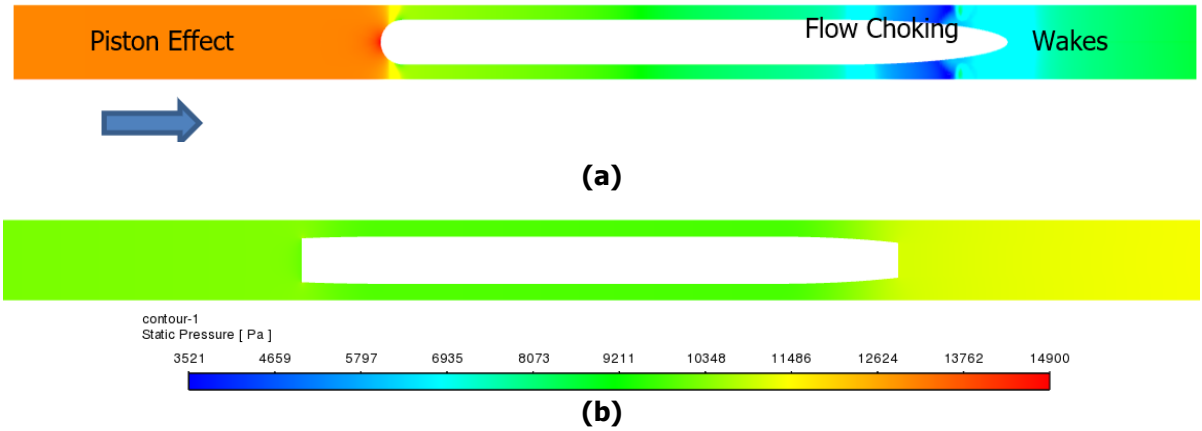

(a)

(b)

Figure 7. Static pressure (a) Blocked, (b) Air-breathed model (M=0.6, P=10 kPa)

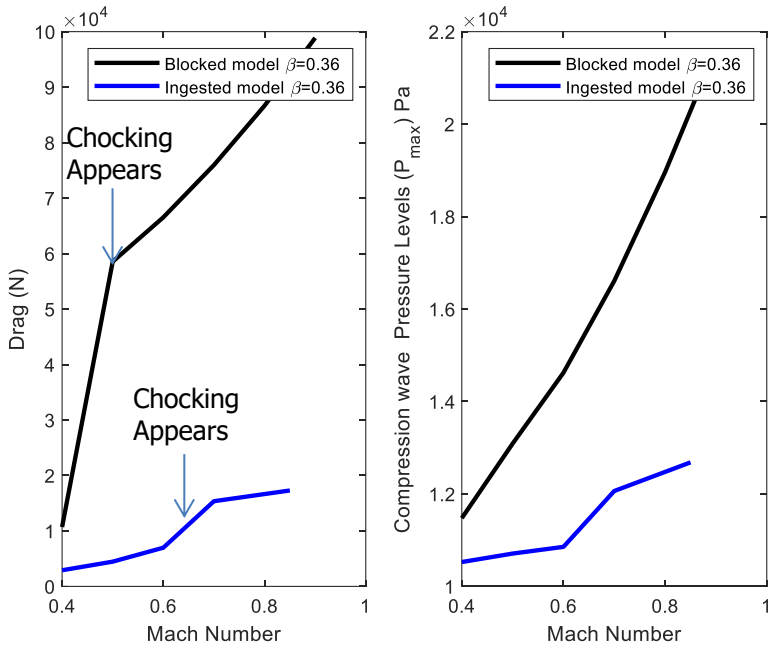

Figure 8. Drag and Piston Pressure variation with Mach number

Fig. (8) reveals that the flow ingestion delays the flow choking. However, the blocked model shows a sharp drag gradient due to the Kantrowitz effect [42], [43]. For ingested model, the chocking appears delayed with respect to the vehicle Mach number allowing moving faster, resulting in a significant reduction in drag and, as a result, lower power consumption at a given blockage ratio of 0.36.

3.3 Effect of ingestion on Mach number distribution

Moving at high speed in closed environments is limited by so-called Kanterwitz limits. The blocked model demonstrated in Fig. (9-a) which faces a choking phenomenon that leads to higher power consumption. Applying flow ingestion, as provided in Fig. (9-b), reduces Mach number levels within the vehicle tube system and hence reducing the shock wave drag.

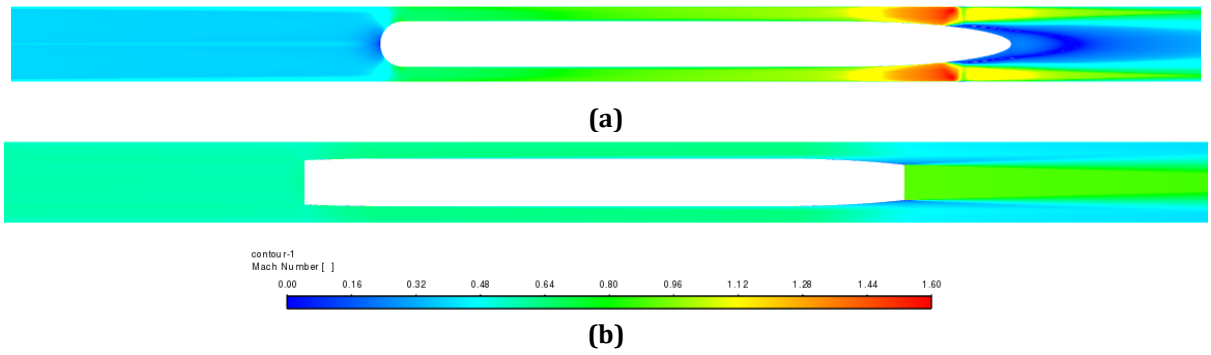

Figure 9. Mach number (a) Blocked, (b) Air-breathed model (M=0.6, p=10 kPa)

3.4 Effect of ingestion on drag

Fig. (10) shows that the blocked model drag force is higher than the ingested model, by using URANS $k-\omega$ SST at (M=0.6 and $\beta = 0.36$). Regarding the drag force components, the pressure drag dominates for the blocked model. However, for the ingested model, the pressure drag is slightly greater than the viscous drag component. It can also be observed that the viscous drag is almost the same for the blocked and ingested models. These results could open the gate for researchers to investigate more on developing air-breathing vehicle-tube systems.

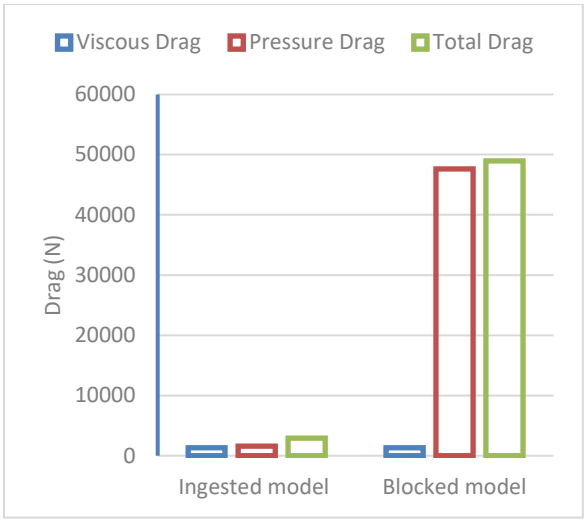

Figure 10. Drag force components for blocked and ingested models (M=0.6, P=10 kPa, $\beta = 0.36$)

3.5 Power analysis for blocked and ingested models

Mitigating the piston effect and converting the tremendous pressure energy into thrust to move the vehicle are the ultimate goals of this work. Certainly, this simplified model requires more investigation to be conducted to emphasize the importance of the ducting system through the pod. The current design presumes using EfanX from Siemens and Rolls-Royce [35]. The process starts by specifying that blockage ratio and Mach number are the key parameters for the design space. The objective is to calculate the drag and power for each design point. The design space was filled with two plans, and the most covering the design space was selected. The flowfield is solved by employing the URANS simulations. The following section describes the developed algorithm for response surface generation. As shown in Fig. (11), the O-kriging [44] was used to study the response surface for the vehicle-tube system with and without flow ingestion. The number of samples extremely affects the computational budget, and the high-resolution response surface also requires increasing the number of design samples. The appropriate method that provides an optimized sampling is the Latin Hypercube method[45], [46].

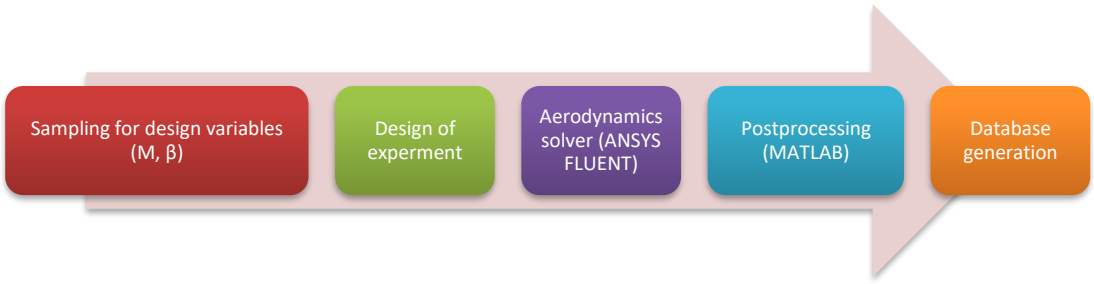

Figure 11. The suggested interactive subroutine

Two sampling plans were studied, and the best filling the design space with a minimum computational budget was selected [47].

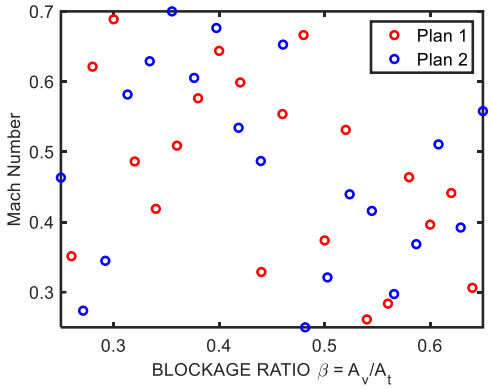

Figure 12. Sampling plans for the design space using Latin Hypercube

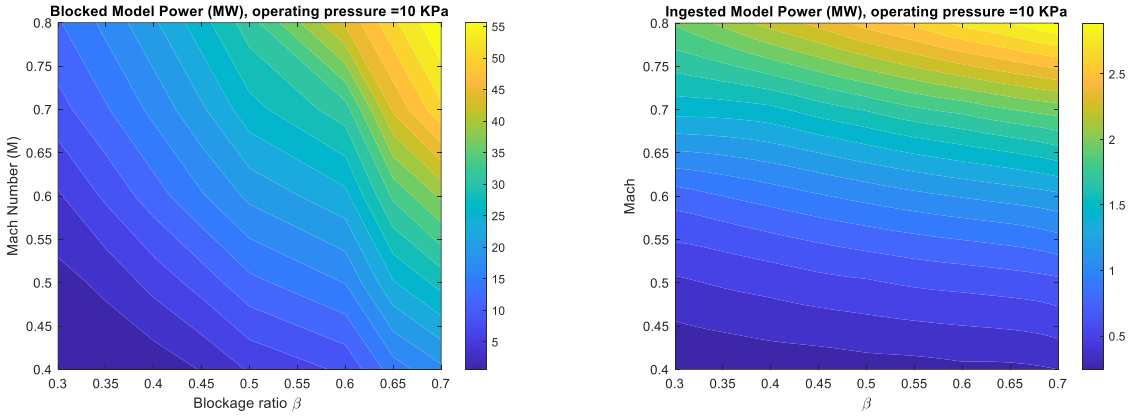

(a) **(b)**

Figure 13. Response surface of power due to drag (a) Blocked & (b) Ingested model

The aerodynamics drag is the primary "friction" force since the maglev system mitigates the friction significantly. The response surface for the power (MW) for the blocked and ingested models are provided in Fig. (13) a and b, respectively. It is obvious that enabling flow ingestion reduces the power magnitude by approximately 10. As a result, the remarkable power reduction will make the operating pressure levels within 10 kPa feasible and attractive. It can be argued that rather than going to very low pressure, allowing flow ingestion inside the pod reduced power consumption remarkably.

3.6 3-D Aerodynamics analysis

The two-dimensional analysis is suitable for the surrogate model described previously for its acceptable computational time (section 3.5). The suggested optimal design point is then investigated using 3D models for the ingested case. The close proximity channel between pod and Maglev is now considered. The blockage ratio of 0.36, which is in agreement with the work of Kim et al. [48]was selected. The $k-\omega$ SST model was utilized with a value of y+ of 5 to investigate the flowfield. Flow Mach number and pressure are studied as illustrated in Fig. (14) at an operating Mach Number of 0.6. It can be shown that the exit nozzle Mach Number is approximately 1.3, which clearly proves the contribution of the ingestion to the overall propulsion of the pod. A boundary layer separation due to strong shock wave-boundary layer interaction in the rear body is presented, requiring careful attention to the aftbody shape.

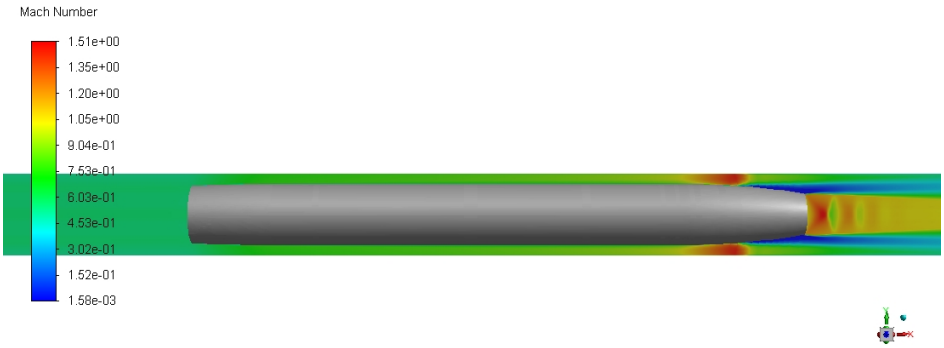

Figure 14. 3D model Mach number contours (M=0.6, $\beta = 0.36$, P=10 kPa)

The static pressure distribution around the vehicle in the confined tube system is illustrated in Fig. (15). The pressure drops downstream due to the velocity increment and the variable area's presence at M=0.6 and $\beta = 0.36$. It is evident that near the aft body in the confined space between tube and pod, there is a flow acceleration that causes a drop in static pressure when the Mach number reaches approximately 1.5, as presented in Fig. (14). The exit nozzle provides lower pressure to maintain the mass flow rate levels, which is defined as a boundary condition. The reflected shockwaves at the jet stream are due to the unity Mach number assigned to the exit nozzle, so careful consideration should be offered to the exit nozzle as it can control the downstream pressure and Mach number levels.

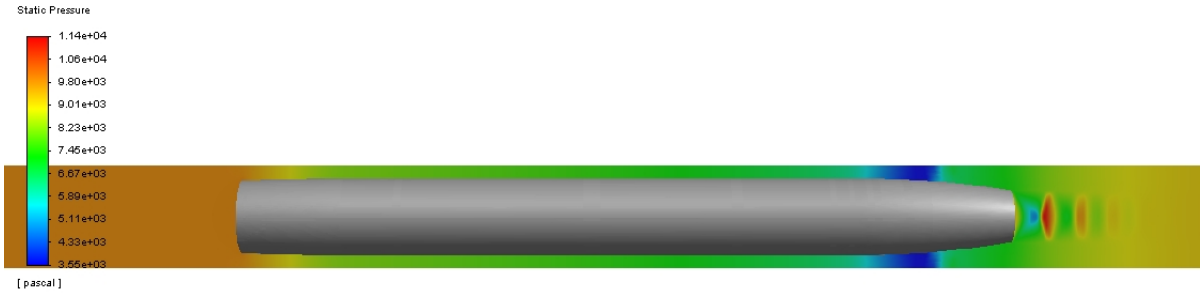

Figure 15. Static Pressure contour (M=0.6, $\beta = 0.36$, P=10 kPa)

4 Conclusion

This work provides some insights into a vehicle moving in a closed low-pressure environment (tube/tunnel). This concept is not to go to ultimate low operating pressure. Although it is quite similar to the hyperloop, a pressure level equal to 10 kPa is well adopted to enhance the safety of the passengers. The study highlights the concept of the flow breathing through the vehicle to contribute to the thrust force required to propel the vehicle. An electrical motor with an axial fan/compressor configuration is introduced to allow the flow ingestion. Since the Efanx is a type certified aero engine working with an electrical motor, it could be a starting point for designers of hyperloop programs.

Multi-dimensional aerodynamics analysis was performed starting from 1-D method of characteristics solution, moving to the 2-D URANS extensive analysis, and eventually to the 3-D analysis of the model using high speed computing unit to study the aerodynamics drag and power consumption applied to different designs and operating conditions. It aims to generate an aerodynamics database for the various configurations considering different flow conditions and design variables with optimized numerical cost using surrogate models.

It has been concluded that the role of ingesting mechanism is evident in reducing the power consumption and propelling the vehicle. Results showed that drag force increases rapidly if the flow chocking phenomenon appears, and the flow ingestion would delay the flow chocking to a higher Mach number. Also, the lowest drag force occurs at β=0.3~0.4. In this paper, the piston effect/compression wave and flow chocking condition are reduced remarkably by considering the ingestion through the vehicle. Further studies and investigations could be devoted to some challenges associated with this kind of system, such as flow separation, transition, and rear-pod flow mixing.

References

[1] E. Musk, "Hyperloop Alpha," *SpaceX/Tesla Motors*, pp. 1–58, 2013, doi: 10.1002/9781119171386.

[2] R H Goddard, "Vaccum Tube Transportation," 1950

[3] J. v Foa, "TRANSFORTATION MEANS AND METHOD," 1965.

[4] D. Oster, M. Kumada, and Y. Zhang, "Evacuated tube transport technologies (ET3)tm: a maximum value global transportation network for passengers and cargo," *Journal of Modern Transportation*, vol. 19, no. 1, pp. 42–50, 2011, doi: 10.1007/bf03325739.

[5] M. M. J. Opgenoord and P. C. Caplan, "Aerodynamic design of the Hyperloop concept," *AIAA Journal*, vol. 56, no. 11, pp. 4261–4270, 2018, doi: 10.2514/1.J057103.

[6] J. Braun, J. Sousa, and C. Pekardan, "Aerodynamic design and analysis of the hyperloop," *AIAA Journal*, vol. 55, no. 12, pp. 4053–4060, 2017, doi: 10.2514/1.J055634.

[7] A. G. HAMMITT, "Unsteady Aerodynamics of Vehicles in Tubes," *AIAA Journal*, vol. 13 NO 4, no. (APRIL 1975), pp. 497–501, 1975.

[8] A. G. Hammitt, "Aerodynamics of Vehicles in Finite Length Tubes.," *Fed Railroad Adm, Off of Res, Dev, and Demonstr, Final Rep FRA-ORD&D-74-10*, no. April, 1974.

[9] P. E. Ross, "Hyperloop: No pressure: The vacuum train project will get its first test track this year," *IEEE Spectrum*, vol. 53, no. 1, pp. 51–54, Jan. 2016, doi: 10.1109/MSPEC.2016.7367468.

[10] H. M. Noh, "Wind tunnel test analysis to determine pantograph noise contribution on a high-speed train," *Advances in Mechanical Engineering*, vol. 11, no. 10, pp. 1–11, 2019, doi: 10.1177/1687814019884778.

[11] M. Yang, J. Du, Z. Li, S. Huang, and D. Zhou, "Moving model test of high-speed train aerodynamic drag based on stagnation pressure measurements," *PLoS ONE*, vol. 12, no. 1, pp. 1–15, 2017, doi: 10.1371/journal.pone.0169471.

[12] X. Zhang, Y. Ge, and J. Sun, "CFD performance analysis of finned-tube CO2 gas coolers with various inlet air flow patterns," *Energy and Built Environment*, vol. 1, no. 3, pp. 233–241, 2020, doi: 10.1016/j.enbenv.2020.02.004.

[13] N. Nick and Y. Sato, "Computational fluid dynamics simulation of Hyperloop pod predicting laminar–turbulent transition," *Railway Engineering Science*, vol. 28, no. 1, pp. 97–111, 2020, doi: 10.1007/s40534-020-00204-z.

[14] M. M. Opgenoord and P. Caplan, "MIT Hyperloop Final Report," *MIT Hyperloop Team*, p. 134, 2017, [Online]. Available: http://web.mit.edu/mopg/www/papers/MITHyperloop_FinalReport_2017_public.pdf

[15] J. S. Oh *et al.*, "Numerical analysis of aerodynamic characteristics of Hyperloop system," *Energies (Basel)*, vol. 12, no. 3, pp. 1–17, 2019, doi: 10.3390/en12030518.

[16] K. Decker *et al.*, "Conceptual feasibility study of the Hyperloop vehicle for next-generation transport," *AIAA SciTech Forum - 55th AIAA Aerospace Sciences Meeting*, no. January, pp. 1–22, 2017, doi: 10.2514/6.2017-0221.

[17] F. Lluesma-Rodríguez, T. González, and S. Hoyas, "CFD simulation of a hyperloop capsule inside a closed environment," *Results in Engineering*, vol. 9, no. December 2020, pp. 2020–2022, 2021, doi: 10.1016/j.rineng.2020.100196.

[18] A. Khayrullina, B. Blocken, W. Janssen, and J. Straathof, "CFD simulation of train aerodynamics: Train-induced wind conditions at an underground railroad passenger platform," *Journal of Wind Engineering and Industrial Aerodynamics*, vol. 139, pp. 100–110, 2015, doi: 10.1016/j.jweia.2015.01.019.

[19] P. Zhou, J. Zhang, T. Li, and W. Zhang, "Numerical study on wave phenomena produced by the super high-speed evacuated tube maglev train," *Journal of Wind Engineering and Industrial Aerodynamics*, vol. 190, no. 111, pp. 61–70, 2019, doi: 10.1016/j.jweia.2019.04.003.

[20] Z. Sajó, L. Benedetti, and N. Riva, "Modeling The Hyperloop With COMSOL Multiphysics®: On The Design Of The EPFLoop Pressurized Systems Zsófia," *Comsol Conference Proceedings*, no. October, pp. 1–7, 2018.

[21] M. M. J. Opgenoord and P. C. Caplan, "On the aerodynamic design of the hyperloop concept," *35th AIAA Applied Aerodynamics Conference, 2017*, no. June, pp. 1–16, 2017, doi: 10.2514/6.2017-3740.

[22] T. Ogawa and K. Fujii, "Numerical investigation of three-dimensional compressible flows induced by a train moving into a tunnel," *Computers and Fluids*, vol. 26, no. 6, pp. 565–585, 1997, doi: 10.1016/S0045-7930(97)00008-X.

[23] R. Janzen, "TransPod Ultra-High-Speed Tube Transportation: Dynamics of Vehicles and Infrastructure," in *Procedia Engineering*, 2017, vol. 199, pp. 8–17. doi: 10.1016/j.proeng.2017.09.142.
[24] Y. Sui *et al.*, "Impact of vacuum degree on the aerodynamics of a high-speed train capsule running in a tube," *International Journal of Heat and Fluid Flow*, vol. 88, no. September 2020, p. 108752, 2021, doi: 10.1016/j.ijheatfluidflow.2020.108752.
[25] R. S. Raghunathan, H.-D. Kim, and T. Setoguchi, "Aerodynamics of high-speed railway train," 2002.
[26] T. K. Kim, K. H. Kim, and H. bin Kwon, "Aerodynamic characteristics of a tube train," *Journal of Wind Engineering and Industrial Aerodynamics*, vol. 99, no. 12, pp. 1187–1196, 2011, doi: 10.1016/j.jweia.2011.09.001.
[27] K. S. Jang, T. T. G. Le, J. Kim, K. S. Lee, and J. Ryu, "Effects of compressible flow phenomena on aerodynamic characteristics in Hyperloop system," *Aerospace Science and Technology*, vol. 117, p. 106970, 2021, doi: 10.1016/j.ast.2021.106970.
[28] H. Kang, Y. Jin, H. Kwon, and K. Kim, "A study on the aerodynamic drag of transonic vehicle in evacuated tube using computational fluid dynamics," *International Journal of Aeronautical and Space Sciences*, vol. 18, no. 4, pp. 614–622, 2017, doi: 10.5139/IJASS.2017.18.4.614.
[29] M. Bizzozero, Y. Sato, and M. A. Sayed, "Aerodynamic study of a Hyperloop pod equipped with compressor to overcome the Kantrowitz limit," *Journal of Wind Engineering and Industrial Aerodynamics*, vol. 218, Nov. 2021, doi: 10.1016/j.jweia.2021.104784.
[30] T. Miyachi, S. Ozawa, T. Fukuda, and M. Iida, "A New Simple Equation Governing Distortion of Compression Wave Propagating Through Shinkansen Tunnel with Slab Tracks," vol. 8, no. 3, pp. 60–73, 2013, doi: 10.1299/jfst.8.462.
[31] T. Miyachi, S. Ozawa, M. Iida, T. Fukuda, and T. Arai, "Propagation characteristics of tunnel compression waves with multiple peaks in the waveform of the pressure gradient: Part 2: Theoretical and numerical analyses," *Proceedings of the Institution of Mechanical Engineers, Part F: Journal of Rail and Rapid Transit*, vol. 230, no. 4, pp. 1309–1317, 2016, doi: 10.1177/0954409715602728.
[32] J. C. Chin, J. S. Gray, S. M. Jones, and J. J. Berton, "Open-source conceptual sizing models for the hyperloop passenger pod," *56th AIAA/ASCE/AHS/ASC Structures, Structural Dynamics, and Materials Conference*, pp. 1–20, 2015, doi: 10.2514/6.2015-1587.
[33] T. Miyachi, S. Saito, T. Fukuda, Y. Sakuma, S. Ozawa, and T. Arai, "Propagation characteristics of tunnel compression waves with multiple peaks in the waveform of the pressure gradient : Part 1 : Field measurements and mathematical model," vol. 0, no. 0, pp. 1–12, 2015, doi: 10.1177/0954409715593305.
[34] T. Miyachi, S. Ozawa, T. Fukuda, and M. Iida, "A New Simple Equation Governing Distortion of Compression Wave Propagating Through Shinkansen Tunnel with Slab Tracks," vol. 8, no. 3, pp. 60–73, 2013, doi: 10.1299/jfst.8.462.
[35] "Our stories | Rolls-Royce - The world's most powerful flying generator." https://www.rolls-royce.com/media/our-stories/discover/2019/e-fan-x-continues-to-explore.aspx (accessed Jul. 19, 2022).
[36] J. C. Chin, J. S. Gray, S. M. Jones, and J. J. Berton, "Open-source conceptual sizing models for the hyperloop passenger pod," *56th AIAA/ASCE/AHS/ASC Structures, Structural Dynamics, and Materials Conference*, pp. 1–20, 2015, doi: 10.2514/6.2015-1587.
[37] C. Liu, K. Xu, and G. Zhou, "Cell Size Effect on Computational Fluid Dynamics: The Limitation Principle for Flow Simulation," pp. 1–35, 2017, [Online]. Available: http://arxiv.org/abs/1706.08200
[38] A. G. Hammitt, "Aerodynamics of Vehicles in Finite Length Tubes.," *Fed Railroad Adm, Off of Res, Dev, and Demonstr, Final Rep FRA-ORD&D-74-10*, no. April, 1974.
[39] A. G. HAMMITT, "Unsteady Aerodynamics of Vehicles in Tubes," *AIAA Journal*, vol. 13 NO 4, no. (APRIL 1975), pp. 497–501, 1975.
[40] A. G. Hammitt, "Aerodynamic analysis of tube vehicle systems," *AIAA Journal*, vol. 10, no. 3, pp. 282–290, 1972, doi: 10.2514/3.6577.
[41] W. A. Woods and C. W. Pope, "A generalised flow prediction method for the unsteady flow generated by a train in a single-track tunnel," *Journal of Wind Engineering and Industrial Aerodynamics*, vol. 7, no. 3, pp. 331–360, May 1981, doi: 10.1016/0167-6105(81)90057-X.

[42] H. Kang, Y. Jin, H. Kwon, and K. Kim, "A study on the aerodynamic drag of transonic vehicle in evacuated tube using computational fluid dynamics," *International Journal of Aeronautical and Space Sciences*, vol. 18, no. 4, pp. 614–622, 2017, doi: 10.5139/IJASS.2017.18.4.614.
[43] F. T. H. Wong, "Aerodynamic design and Optimization of a Hyperloop Vehicle," TU Delft, 2018.
[44] M. A. Bouhlel and J. R. R. A. Martins, "Gradient-enhanced kriging for high-dimensional problems," *Engineering with Computers*, vol. 35, no. 1, pp. 157–173, 2019, doi: 10.1007/s00366-018-0590-x.
[45] D. Gorissen, I. Couckuyt, P. Demeester, T. Dhaene, and K. Crombecq, "A surrogate modeling and adaptive sampling toolbox for computer based design," *Journal of Machine Learning Research*, vol. 11, pp. 2051–2055, 2010.
[46] P. S. Palar, R. P. Liem, L. R. Zuhal, and K. Shimoyama, "On the use of surrogate models in engineering design optimization and exploration," no. May, pp. 1592–1602, 2019, doi: 10.1145/3319619.3326813.
[47] C.-H. Chen and L. H. Lee, "Computing Budget Allocation," *Stochastic Simulation Optimization*, pp. 15–28, 2010, doi: 10.1142/9789814282659_0002.
[48] T. K. Kim, K. H. Kim, and H. bin Kwon, "Aerodynamic characteristics of a tube train," *Journal of Wind Engineering and Industrial Aerodynamics*, vol. 99, no. 12, pp. 1187–1196, 2011, doi: 10.1016/j.jweia.2011.09.001.